Photosynth Res (2017) 133:185–199
DOI 10.1007/s11120-017-0366-y

ORIGINAL ARTICLE

Kinetic modeling of electron transfer reactions in photosystem I complexes of various structures with substituted quinone acceptors

Georgy E. Milanovsky[1] · Anastasia A. Petrova[1] · Dmitry A. Cherepanov[1,2] · Alexey Yu. Semenov[1,3]

Received: 21 November 2016 / Accepted: 1 March 2017 / Published online: 28 March 2017

Abstract The reduction kinetics of the photo-oxidized primary electron donor P_{700} in photosystem I (PS I) complexes from cyanobacteria *Synechocystis* sp. PCC 6803 were analyzed within the kinetic model, which considers electron transfer (ET) reactions between P_{700}, secondary quinone acceptor A_1, iron-sulfur clusters and external electron donor and acceptors – methylviologen (MV), 2,3-dichloro-naphthoquinone (Cl_2NQ) and oxygen. PS I complexes containing various quinones in the A_1-binding site (phylloquinone PhQ, plastoquinone-9 PQ and Cl_2NQ) as well as F_X-core complexes, depleted of terminal iron–sulfur F_A/F_B clusters, were studied. The acceleration of charge recombination in F_X-core complexes by PhQ/PQ substitution indicates that backward ET from the iron–sulfur clusters involves quinone in the A_1-binding site. The kinetic parameters of ET reactions were obtained by global fitting of the P_{700}^+ reduction with the kinetic model. The free energy gap ΔG_0 between F_X and F_A/F_B clusters was estimated as −130 meV. The driving force of ET from A_1 to F_X was determined as −50 and −220 meV for PhQ in the *A* and *B* cofactor branches, respectively. For PQ in A_{1A}-site, this reaction was found to be endergonic ($\Delta G_0 = +75$ meV). The interaction of PS I with external acceptors was quantitatively described in terms of Michaelis–Menten kinetics. The second-order rate constants of ET from F_A/F_B, F_X and Cl_2NQ in the A_1-site of PS I to external acceptors were estimated. The side production of superoxide radical in the A_1-site by oxygen reduction via the Mehler reaction might comprise ≥0.3% of the total electron flow in PS I.

Keywords Photosystem I · Electron transfer · Kinetic modeling · Midpoint redox potentials · External electron acceptor · Superoxide radical production

Abbreviations

PS I	Photosystem I
P_{700}	A special pair of chlorophyll molecules
MV	Methylviologen
Cl_2NQ	2,3-Dichloro-1,4-naphthoquinone
PhQ	Phylloquinone
PQ	Plastoquinone-9
Chl	Chlorophyll
ET	Electron transfer
DCPIP	2,6-Dichlorophenolindophenol
E_m	Midpoint redox potential
WT	Wild type
menB-PQ/*menB*-Cl_2NQ	PS I mutant *menB* with PQ/Cl_2NQ in the A_1-site
ROS	Reactive oxygen species
Fd	Ferredoxin
Fld	Flavodoxin

✉ Dmitry A. Cherepanov
cherepanov@belozersky.msu.ru

✉ Alexey Yu. Semenov
semenov@genebee.msu.ru

[1] A.N. Belozersky Institute of Physical-Chemical Biology, Moscow State University, Moscow, Russia

[2] A.N. Frumkin Institute of Physical Chemistry and Electrochemistry, Russian Academy of Sciences, Moscow, Russia

[3] N.N. Semenov Institute of Chemical Physics, Russian Academy of Sciences, Moscow, Russia

Introduction

Photosystem I (PS I) is a key pigment–protein complex of the electron transfer (ET) chain of oxygenic photosynthetic organisms. It includes both a large antenna system for harvesting solar energy and a photochemical reaction center catalyzing charge separation across the membrane dielectric (for reviews, see Brettel and Leibl 2001; Fromme and Mathis 2004; Mamedov et al. 2015). The X-ray crystallographic structure of the cyanobacterial PS I has been resolved to 2.5 Å resolution (Jordan et al. 2001). The membrane-embedded core of each PS I monomer is formed by the two largest subunits, *PsaA* and *PsaB*, which bind ET cofactors arranged in two symmetrical branches, *A* and *B*, extending from P_{700}, a pair of chlorophyll (Chl) *a* molecules located on the lumenal side, to the [4Fe–4S] cluster F_X, placed on the opposite stromal side of the complex (see Fig. 1). Each of the two branches, related by a pseudo-C_2 rotation axis which passes through P_{700} and F_X, carries two electronically coupled Chl *a* molecules (termed A_{0A} or A_{0B}) and one phylloquinone (PhQ) A_{1A} or A_{1B}. At room temperature (RT), both branches are thought to be active in ET (Guergova-Kuras et al. 2001) (for reviews, see Santabarbara et al. 2005; Srinivasan and Golbeck 2009 and references therein) with the ratio ~80:20% in favor of branch *A* in cyanobacterial PS I (Milanovsky et al. 2014; Sun et al. 2014; Makita and Hastings 2015). The terminal [4Fe–4S] clusters, F_A and F_B, are both bound to the peripheral protein subunit *PsaC*.

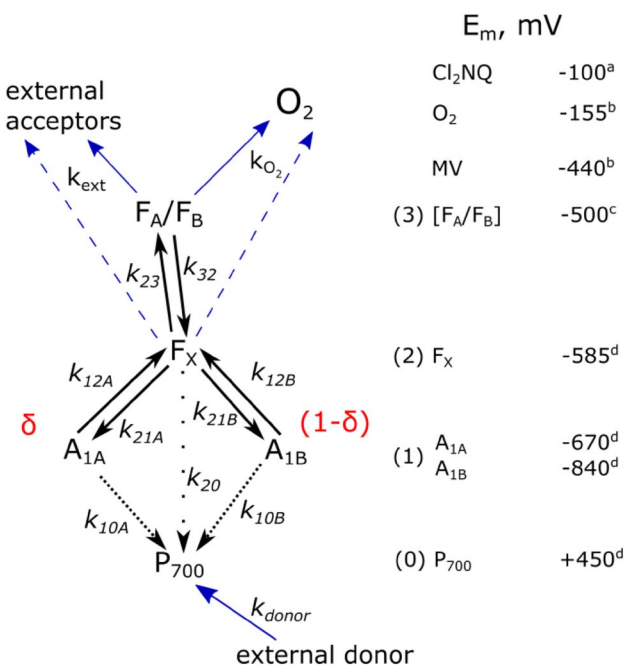

Fig. 1 Kinetic model of PS I, used for interpretation of P_{700}^+ recombination transient changes. ET within PS I protein complex indicated—by *black arrows*; and interaction of PS I with external donor and acceptors indicated—by *blue arrows*. P_{700}^+ recombination transitions are marked by *dotted lines*. Reaction rate constants are noted with *italic lowercase letters* k_i. Direct interaction of F_X with external electron acceptors is considered only for F_X-core complexes (*dashed lines*). Approximate redox potentials of cofactors involved in different steps of charge separation (indexed from 0 to 3) and external acceptors are shown on the *right side*. The midpoint potential (E_m) values were taken from *a* Currie and Holmes (1966); *b* Wardman (1989); *c* Golbeck et al. (1987); *d* Ptushenko et al. (2008)

Upon light excitation, the excited singlet state of the primary electron donor, P_{700}^* delivers an electron to the primary Chl acceptor A_{0A}/A_{0B} forming the charge-separated state $P_{700}^+A_0^-$. The electron is then transferred in sequence to A_{1A}/A_{1B}, to the iron–sulfur cluster F_X, and ultimately to F_A/F_B. When exogenous electron acceptors are not available, the electron on $[F_A/F_B]^-$recombines with the hole on P_{700}^+ with lifetime of 30–100 ms, the charge recombination of $P_{700}^+F_X^-$ pair in the absence of F_A/F_B occurs within lifetime of 0.5–5 ms, and the recombination of $P_{700}^+A_1^-$ (in the absence of all iron–sulfur clusters) takes place within ~100 μs (Vassiliev et al. 1997; Brettel and Leibl 2001; Srinivasan and Golbeck 2009).

While the free energy gap ΔG for ET between A_0 and A_1 was estimated as >420 meV, the ΔG values of further ET events involving 4Fe–4S clusters are about 200 meV (Santabarbara et al. 2005; Ptushenko et al. 2008; Srinivasan and Golbeck 2009). At room temperature, the forward ET from A_1 to F_X follows two alternative pathways. Reaction in the branch *A* has τ of ~300 ns and the activation energy of 110 meV, whereas ET from A_{1B} to F_X is a fast, nearly temperature-independent process (τ of 11–17 ns) (Agalarov and Brettel 2003; Sun et al. 2014). The recombination of $P_{700}^+F_X^-$ is thermally activated, and it evidently follows via the intermediate $P_{700}^+A_1^-$ state (Brettel and Leibl 2001; Shinkarev 2006). Recombination from the F_A/F_B clusters was found to be temperature dependent with an activation energy of ~200 mV (Jordan et al. 1998).

The suppression of the *menA* and *menB* genes, which code for dihydroxynaphthoic acid synthase and phytyltransferase, respectively, results in the termination of PhQ biosynthesis. PS I complexes isolated from *menA* and *menB* mutants contain plastoquinone-9 (PQ) rather than PhQ in the A_1-site and show altered rates of forward ET from A_1^- to $[F_A/F_B]$ and altered rates of back ET from $[F_A/F_B]^-$ to P_{700}^+ (Semenov et al. 2000).

Biochemical processes in thylakoid membranes and stroma of chloroplasts are organized in a complex system of regulatory feedbacks, which require kinetic modeling for quantitative analysis (Matsuoka et al. 2016). PS I is the key element of the energy-transducing pathways because the electron flow in thylakoids is controlled by the redox states of cofactors in the acceptor part of PS I (see Tikhonov 2016 for the recent review). Therefore, the development of proper models of PS I functioning, and the refinement

of midpoint potentials of redox cofactors, is crucial for the quantitative analysis of primary photosynthetic processes.

The modeling of the P_{700} charge recombination kinetics with PhQ and PQ in the A_1-site of PS I was carried out by Shinkarev et al. (2002). The kinetics of flash-induced P_{700}^+ reduction in PS I that contained either an intact set or a subset of iron-sulfur clusters F_X, F_A, and F_B and with the A_1-binding site occupied by PhQ or PQ was studied. A modeling of the forward and backward ET kinetics in P_{700}–F_A/F_B complexes, P_{700}–F_X cores, and P_{700}–A_1 cores showed that the replacement of PhQ by PQ induced a decrease in the free energy gap between A_1 and F_A/F_B from −205 mV in wild-type (WT) PS I to −70 mV in *menA* PS I. The acceleration in the rate of P_{700}^+ dark reduction in *menA* PS I was ascribed to 135 mV increase in the midpoint potential of A_1, thus making ET from A_1 to F_X thermodynamically unfavorable. However, the existence of two alternative ET pathways was not considered in this study.

The modeling of the bidirectional ET reactions in PS I was performed by Santabarbara et al. (2005), and later expanded in (Makita and Hastings 2016; Santabarbara and Zucchelli 2016); however, the thermodynamic parameters used in these studies were largely arbitrary. The ET reactions within PS I were analyzed in terms of Marcus theory, assuming a possibility of ET between the two tightly bound phylloquinones via the iron–sulfur cluster F_X. In this study, the redox potentials of the quinones in the A_1-site were estimated to be almost isoenergetic with that of the iron–sulfur center F_X. More recently, detailed kinetic model was constructed and applied to the transient dynamics of radical pair states in PS I with eight different quinones incorporated into the A_1-binding site at 298 and 77 K (Makita and Hastings 2016). This model indicated that forward ET from A_1^- to F_X in the WT PS I can only be slightly endergonic/exergonic in the *A and B* branches, respectively. In this model, the redox midpoint potential (E_m) of F_X was set at −680 mV, based on the equilibrium redox titration of F_X in PS I (Chamorovsky and Cammack 1982; Parrett et al. 1989). However, the authors in both studies (Santabarbara et al. 2005; Makita and Hastings 2016) did not take into account that the operating midpoint potential of F_X is ~70 mV more positive than the equilibrium E_m value (Ptushenko et al. 2008).

The analysis of ET rates employed in Makita and Hastings (2016), Santabarbara and Zucchelli (2016) was based on the semiclassical approximation developed by Hopfield (1974):

$$k_{DA} = \frac{\sqrt{2\pi}}{\hbar\sigma(T)}|H_{DA}|^2 \exp\left(-\frac{(\Delta G_0 + \lambda)^2}{2\sigma(T)^2}\right) \quad (1)$$

where H_{DA} is the electronic coupling matrix element, ΔG_0 is the standard free energy gap of reaction, λ is the reorganization energy of reaction, and the parameter $\sigma(T)$ is defined as

$$\sigma(T)^2 = \lambda\hbar\omega_0 \coth\frac{\hbar\omega_0}{2k_B T}. \quad (2)$$

As shown by Jortner (1976), this approximation is inadequate for the description of ET reactions in low and intermediate temperature ranges. In particular, the ratio of forward and reverse rate constants in (1) does not satisfy the general thermodynamic relationship $k_{DA}/k_{AD} = \exp(-G_0/k_BT)$.

The study by Santabarbara and Zucchelli (2016) acknowledges that the same experimental kinetic data can be described both by isoenergetic model (used in their previous study) and by a model assuming large driving force of $A_1 \rightarrow F_X$ electron transfer, based on semicontinuum electrostatic calculations of redox potentials of PS I cofactors (Ptushenko et al. 2008).

We have previously demonstrated that molecular oxygen and the oxidized form of ascorbate can accept electrons from PS I complexes containing PQ and 2,3-dichloro-1,4-naphthoquinone (Cl_2NQ) in the A_1-binding site under steady-state illumination (Trubitsin et al. 2014). In this study, we characterize quantitatively the participation of two external acceptors – methylviologen (MV) and Cl_2NQ – in ET reactions in different PS I complexes. In particular, we have studied the interaction of external acceptors with (i) PS I complexes from the WT containing PhQ, (ii) complexes depleted of F_A/F_B clusters (F_X-core), and (iii) the complexes from *menB* mutant strain contained in the A_1-site PQ (*menB*-PQ) and Cl_2NQ (*menB*-Cl_2NQ).

The kinetic modeling in this work was based on the experimentally observed kinetics of P_{700}^+ reduction measured by absorption changes at 820 nm in various PS I complexes in the presence of different concentrations of MV and Cl_2NQ. The experimental data are described in our preceding paper published in the same issue of this Journal (Petrova et al., Photosynt Res, in press).

Model development

The scheme of ET reactions in PS I complexes is presented in Fig. 1. The secondary ion-radical pair $P_{700}^+A_1^-$ is considered as the initial state for kinetic modeling, with the fraction of electrons δ localized at the quinone-binding site A_{1A} in the branch *A* of cofactors, and the fraction $(1-\delta)$ at the site A_{1B} in the branch *B*. The ET kinetics in PS I are described by the following system of differential equations:

$$\frac{d[A_{1A}]}{dt} = k_{21A}[F_X] - (k_{12A} + k_{10A})[A_{1A}]$$

$$\frac{d[A_{1B}]}{dt} = k_{21B}[F_X] - (k_{12B} + k_{10B})[A_{1B}]$$

$$\frac{d[F_X]}{dt} = k_{12A}[A_{1A}] + k_{12B}[A_{1B}] + k_{32}\left[\frac{F_A}{F_B}\right] - \left(k_{21A} + k_{21B} + k_{23} + k_{20}\right)[F_X]$$

$$\frac{d[F_A/F_B]}{dt} = k_{23}[F_X] - \left(k_{32} + k_{O_2} + k_{ext}\right)\left[\frac{F_A}{F_B}\right]$$

$$\frac{d[P_{700}{}^+]}{dt} = -k_{10A}[A_{1A}] - k_{10B}[A_{1B}] - k_{donor}[P_{700}{}^+]$$

where k_{ij} are rate constants of the monomolecular reactions of ET from cofactor i to cofactor j; the indexes 0, 1, 2, and 3 correspond to the P_{700}, A_1, F_X, and $[F_A/F_B]$, respectively; k_{donor} is the rate of $P_{700}{}^+$ reduction by external donor (2,6-dichlorophenolindophenol, DCPIP); k_{O2} is the rate constant of ET to external molecular oxygen in solution. The rates of forward ET reactions from Fe–S clusters to external acceptors k_{ext} were described by Michaelis–Menten equation, where the reaction rate is dependent on the external acceptor concentration [EA] as

$$k_{ext} = \frac{V_m}{K_m}\frac{[EA]}{1 + \frac{[EA]}{K_m}} \quad (3)$$

where V_m is the maximal reaction rate and K_m is the Michaelis constant (e.g., the dissociation constant of external acceptor in the PS I complex). At $[EA] \ll K_m$, the reaction rate is a linear function of acceptor concentration, so the parameter $k_a = V_m/K_m$ could be considered as a pseudo-bimolecular effective rate constant.

It should be noted that the direct recombination between $[F_A/F_B]^-$ and $P_{700}{}^+$ is extremely slow due to a very large distance between the cofactors of >40 Å corresponding to the ET rate of over 10^{-9} s^{-1}, according to Moser–Dutton empirical ruler (Dutton et al. 1999); thus, the experimentally observed slow recombination component, usually attributed to the $P_{700}{}^+[F_A/F_B]^-$ recombination, in fact, represents several consequent ET steps from $[F_A/F_B]^-$ to F_X and most probably to A_1, before recombining with $P_{700}{}^+$ (Sétif et al. 1984; Brettel and Golbeck 1995). Therefore, the experimentally observable $P_{700}{}^+[F_A/F_B]^-$ recombination rate k_{30} can be expressed in terms of two intermediary equilibrium constants K_{ij}:

$$k_{30} = {K_{23}}^{-1}{K_{12A}}^{-1}k_{10A} \quad (4)$$

$$K_{12A} = \frac{k_{12A}}{k_{21A}} \quad (5)$$

$$K_{23} = \frac{k_{23}}{k_{32}} \quad (6)$$

Only the recombination through A branch of cofactors was considered, since the redox potential of A_{1B} is supposed to be at least 100 mV lower than that of A_{1A} (Ishikita and Knapp 2003; Ptushenko et al. 2008), making $F_X{}^- \rightarrow A_{1B}{}^-$ back ET route much less probable than that for $F_X{}^- \rightarrow A_{1A}{}^-$ (see redox potentials of F_X, A_{1A} and A_{1B} in Fig. 1). In addition, the recombination kinetics in F_X-core samples contained small (~17%) sub-millisecond components, which were assigned to the fraction of PS I complexes lacking all Fe–S clusters. In this fraction, no forward ET beyond A_1 occurred, and only the recombination from A_1 cofactors was taken into account. Kinetic model was numerically solved by Runge–Kutta–Fehlberg method (Fehlberg 1970) and fitted to the experimental data using a set of developed scripts for MATLAB, with the gradually increasing number of unrestrained variables.

Basic recombination kinetics analysis

Recombination kinetics of charges appearing in PS I after photo-induced electron emission from the excited primary donor P_{700} cover a wide time range of 10^{-6}–10^{-1} s, and can be approximated by a sum of several exponential components. The redox cofactor chains in PS I are arranged in such a way that the forward ET reactions are much faster than the backward reactions, so the recombination kinetics may be particularly informative in modified PS I complexes where the intermediate stages could be resolved. As an illustration of how kinetic parameters of forward and backward reactions can be derived from the recombination kinetics, the following kinetic scheme is considered:

$$D^+ \xleftarrow{k_{10}} A_1 \underset{k_{21}}{\overset{k_{12}}{\longleftrightarrow}} A_2 \quad (7)$$

At zero time, the electron is located at the acceptor A_1, and its subsequent redistribution between cofactors is determined by three rate constants, with general relationship $k_{12} \gg k_{21}$, k_{10}. The typical kinetics of donor D reduction is shown in Fig. 2, which comprises two exponential components. The characteristic time of the faster component is determined by the sum of forward and backward rate constants (red line in Fig. 2):

$$\tau_1 = \left(k_{12} + k_{10}\right)^{-1} \approx {k_{12}}^{-1},$$

where the characteristic time of the slow component is determined by the recombination rate constant k_{10} multiplied by the equilibrium constant $K_{12} = k_{12}/k_{21}$ (green line in Fig. 2):

$$\tau_2 = K_{12}{k_{10}}^{-1}$$

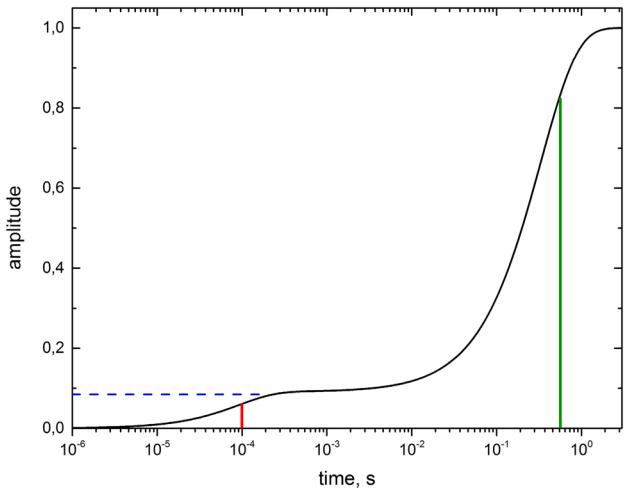

Fig. 2 The recombination kinetics in the three-state ET model. The ordinate *axis* shows the fraction of reduced donor *D*

Amplitude of the faster component (*blue line* in Fig. 2) is determined by the expression:

$$a_1 = \frac{k_{10}}{k_{12} + k_{10}}.$$

Thus, the kinetics of the electron donor *D* reduction allows determining explicitly the rate constants of the forward $A_1 \rightarrow A_2$ and both reverse reactions: $A_2 \rightarrow A_1$ and $A_1 \rightarrow D$. The free energy change ΔG_{12} for electron distribution between acceptors A_1 and A_2 in equilibrium is

$$\Delta G_{12} = -RT \ln(k_{12}/k_{21}). \quad (8)$$

Results of kinetic modeling

Kinetic parameters, obtained by straight assessment of experimental data with the kinetic model shown in Fig. 1, are marked in Table 1 in bold. Some parameters of the model are known from literature and were taken as following. The rate constants k_{12A} and k_{12B} of forward ET from A_1 to F_X were 5×10^6 and 5×10^7 s^{-1} for branches *A* and *B*, respectively (Setif and Brettel 1993; Guergova-Kuras et al. 2001). The estimate constant $K_{12B} = 1.8\times10^4$ was taken from the previously calculated difference between midpoint potentials of A_{1B} and F_X (Ptushenko et al. 2008). The rate constant k_{23} of forward ET from F_X to F_A/F_B was taken as 10^7 s^{-1}, based on the fact that the forward ET reactions in PS I are limited by $A_{1A} \rightarrow F_X$ stage and not by further ET steps (Díaz-Quintana et al. 1998). The asymmetry factor δ was assumed to be ~80% (Sun et al. 2014; Makita and Hastings 2015).

The observed rate of recombination from terminal F_A/F_B clusters, k_{30}, does not represent a direct ET reaction, but rather a series of ET events (see Eqs. 4–6). The observed acceleration of charge recombination in *menB*-PQ indicates that backward ET from the terminal iron–sulfur clusters occurred via A_1 (see "Discussion" below), and the rate constant k_{20} of direct recombination from F_X cluster was zero. Thus, we determined, at first, the value of K_{12A} from F_X-core kinetics, where ET beyond F_X was not observed, and then K_{23} was estimated for the WT complex, assuming the same K_{12A} value. In *menB*-PQ complex, conversely, the value of K_{23} is expected to be the same as that in the WT complex, while K_{12A} decreases due to the more positive redox potential of A_1 compared with the WT PS I. The values of recombination rate constants k_{10A} and k_{10B} for quinones in branches, *A* and *B*, respectively, were determined for F_X-core and *menB*-Cl_2NQ systems and were assumed to be the same as those in the WT as in F_X-core. The rates of ET to P_{700}^+ from external donor DCPIP, k_{donor}, slightly varied in different experiment series due to adjustable DCPIP concentrations and are not presented in Table 1.

Recombination kinetics in PS I of WT

The recombination of P_{700}^+ in the WT PS I with varying concentrations of methylviologen is presented in Fig. 3. Without external acceptor, ~60% of electrons are transferred to molecular oxygen (red dotted line 4), whereas the internal recombination with P_{700}^+ passes through the quinone A_{1A} (the recombination via A_{1B} is <5%, the combined recombination from terminal acceptors via both quinones is shown by black dashed line 2). With the increasing concentration of MV, the electron flow is captured by this acceptor, reaching ~90% at 10 μM of MV (blue dotted line 6). The kinetic parameters for intrinsic ET reactions are given in Table 1, and for external ET reactions in

Table 1 Kinetic and thermodynamic parameters of intrinsic ET reactions in PS I

System	k_{12A}, s^{-1}	k_{12B}, s^{-1}	k_{30}, s^{-1}	K_{12A}	K_{23}	$K_{12A}\times K_{23}$	k_{10A}, s^{-1}	k_{10B}, s^{-1}
WT	5×10^6	5×10^7	**7.6**	7	170	1200	9.1×10^3	4×10^5
F_X-core	5×10^6	5×10^7	$\mathbf{1.3\times10^3}$	7	–	–	$\mathbf{9.1\times10^3}$	$\mathbf{4\times10^5}$
menB-PQ	$\mathbf{1.4\times10^4}$	$\mathbf{3\times10^5}$	**325**	0.05	170	**8.5**	$\mathbf{2.5\times10^3}$	$\mathbf{5\times10^4}$
menB-Cl_2NQ							$\mathbf{9.3\times10^3}$	$\mathbf{2.8\times10^5}$

See Fig. 1 for rate constants k_{ij} and Eqs. 4–6 for equilibrium constants K_{ij}. Kinetic parameters, obtained by straight assessment of experimental data with the kinetic model, are marked in bold

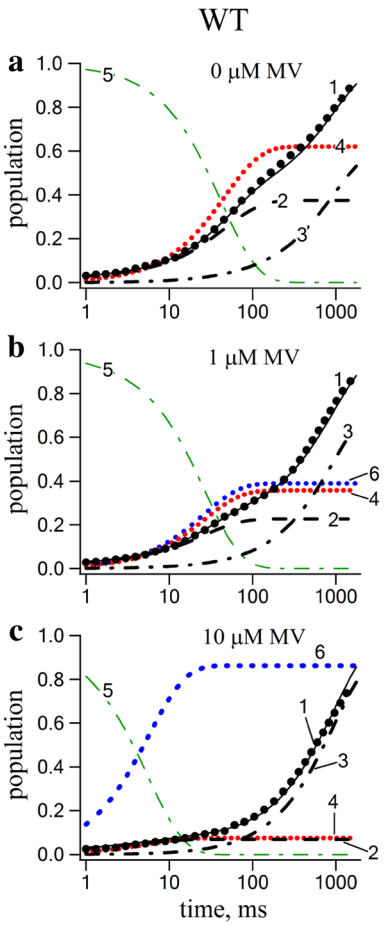

Fig. 3 Effect of MV as external acceptor on the P_{700}^+ reduction in WT PS I. Curves notation: experimental P_{700} recovery kinetics (*black dots*, 1), modeled P_{700} recovery kinetics (*black solid line*, 1); the fraction of P_{700} population, reduced by terminal acceptors (*black dashed line*, 2) and by external donor DCPIP (*black dash-dotted line*, 3); the reduced external oxygen (*red dotted line*, 4); the population of reduced iron–sulfur clusters (thin *green dash-dotted line*, 5); and the reduced external acceptor MV (*blue dotted line*, 6)

Table 2, respectively. The recombination kinetics in WT PS I without MV are similar to the data obtained in previous experiments (Shinkarev et al. 2000; Makita and Hastings 2016) and could serve as a reference point for further modeling. Similar kinetics were obtained for PS I with varying concentrations of Cl_2NQ as an external electron acceptor (Fig. 4). Cl_2NQ is more efficient than MV, accepting 40% of the total electron flow at concentration of 0.25 μM (Fig. 4b), whereas the similar effect was observed at ~1 μM MV (Fig. 3b).

Recombination kinetics in F_X-core

The recombination kinetics in the F_X-core complexes lacking F_A/F_B clusters in the presence of MV (Fig. 5) differs from the recombination in WT PS I in two respects. (i) The main component of recombination kinetics is much faster than in the WT ($\tau \approx 1$ ms instead of >10 ms), so the ET to oxygen is less pronounced than in the WT, contributing <15% to the total amplitude in the absence of MV and even less in the presence of external electron acceptor. At the maximal MV concentration (1000 μM), the external acceptor captures ~60% of electrons, whereas this reaction reaches ~100% in the case of WT. (ii) In the F_X-core preparations, there are minor recombination components with the lifetimes in the range of 1–10 μs, which are probably related to damaged complexes depleted of all Fe–S clusters, where the direct recombination from A_{1A}/A_{1B} occurs. The model fitting in accordance with this assumption yielded the fraction of such damaged complexes to be ~17%.

As in the case of WT PS I, in F_X-core complexes Cl_2NQ functioning as external acceptor demonstrated a behavior similar to MV (Fig. 6). However, Cl_2NQ was tenfold more efficient compared with MV: Cl_2NQ at 100 μM and MV at 1000 μM demonstrated similar rates of electron capture. Both acceptors were unable to completely remove the intermediate recombination component ($\tau \leq 1$ ms), capturing ~60% of electrons at the maximal acceptor concentrations.

Recombination kinetics in PS I with PQ and Cl_2NQ in the A_1-site

Electron recombination in *menB*-PQ complexes is much faster than that in the WT, where its main component has τ of ~3 ms. This component disappeared upon MV addition as in the case of the WT (Fig. 7). Since *menB* mutant contains the same set of terminal cofactors as the WT, the acceleration of charge recombination could be explained by a higher E_m of PQ in the A_1-site, e.g., the electron recombination from terminal F_A/F_B clusters occurs sequentially via the intermediate ET to A_1, but not directly to P_{700}.

We were unable to approximate the recombination kinetics of *menB*-Cl_2NQ system with the same kinetic model as three other systems, where external acceptors capture electrons from the Fe–S clusters. Alternatively, a model considering direct ET to external acceptors from A_1 was shown to be more consistent with the experimental data (Fig. 8). Two asymmetric cavities can be found in crystallographic structure of PS I (Jordan et al. 2001) within ~10 Å from the phylloquinone molecules in the A_1-site, dimensions of which are close to those of MV (Fig. 9). Thus, MV might bind to PS I in the vicinity of Cl_2NQ in the A_1-site, which provides direct transfer of an electron from A_1 to MV. The detailed study of this process could be the focus of another study utilizing molecular dynamics, which is currently considered in our laboratory. Therefore, the slow component of P_{700} recombination in *menB*-Cl_2NQ system, diminishing with the increasing MV concentration, was attributed to A_{1A} recombination with P_{700}^+ (black solid line 2), which

Table 2 Parameters of PS I interactions with external acceptors, according to kinetic model. See section "Model development" for definition of effective rate constant k_a

System	Interaction with external acceptor	
	Michaelis constant K_m, M	k_a, M^{-1} s^{-1}
MV		
WT	$\gg 10^{-4}$	1.6×10^{7}
F_X-core	$\gg 10^{-3}$	5.2×10^{6}
menB-PQ	$\gg 10^{-4}$	2×10^{7}
menB-Cl_2NQ	10^{-5}	1.5×10^{9}
Cl_2NQ		
WT	5.2×10^{-6}	1.1×10^{8}
F_X-core	$\gg 10^{-4}$	5×10^{7}
O_2		
WT	n.d	7.5×10^{4}
F_X-core	n.d	1.2×10^{6}
menB-PQ	n.d	2×10^{5}
menB-Cl_2NQ	n.d	5×10^{6}
*Fd**		
WT	4×10^{-7}	3.5×10^{8}
*Fld**		
WT	7.5×10^{-6}	3.6×10^{7}

*The K_m and k_a values for native acceptor proteins ferredoxin (*Fd*) and flavodoxin (*Fld*) were taken from (Setif 2001)

competes with the electron withdrawal by MV (blue dotted line 8). As the faster recombination component (~10 µs, black solid line 3) is not affected by MV, it could be concluded that recombination between A_{1B}^- and P_{700}^+ occurs faster than the potential electron donation to MV.

Parameters of PS I interaction with external acceptors MV and Cl_2NQ, according to reaction rates determined within the kinetic model, are summarized in Table 2. The dissociation constant K_m of the protein–acceptor complex and the effective second-order reaction rate constant k_a (equal to V_{max}/K_m, where V_{max} is the maximal reaction rate, see Eq. 3) are shown. Only for two systems, namely, *menB*-Cl_2NQ with MV as external acceptor and F_X-core with Cl_2NQ as external acceptor, the values of K_m were determined, as in all other cases, the reaction rates linearly depended on external acceptor concentration. The maximal acceptor concentrations used in the experiments are presented in the respective cells of Table 2 as the lower bound of K_m values. It should be noted that for *menB*-Cl_2NQ direct, ET from A_{1A} to external acceptor is considered, whereas in all other cases, the parameters are related to ET from the terminal 4Fe–4S clusters.

Reaction rates k_a for MV as external acceptor in WT and *menB*-PQ systems were similar, as expected (1.6×10^7 and 2×10^7 s^{-1}, respectively), whereas for F_X-core a lower value of 5.2×10^6 s^{-1} was obtained. Reaction rates for Cl_2NQ as external acceptor were approximately an order of magnitude higher than those for MV.

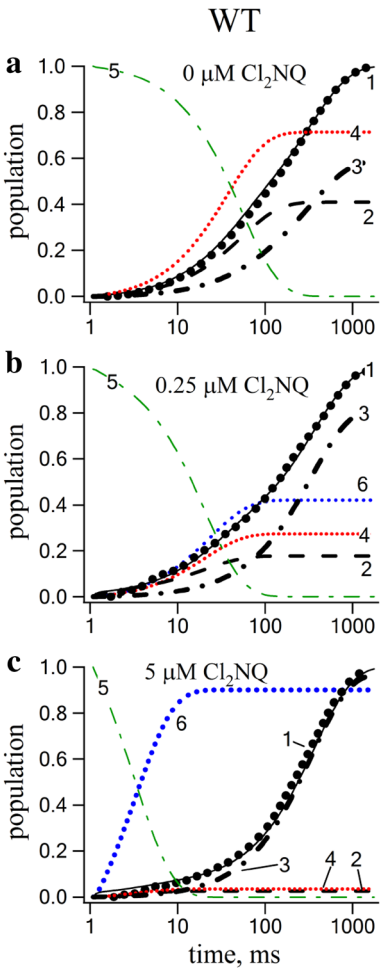

Fig. 4 Effect of Cl_2NQ on the P_{700}^+ reduction in WT PS I. The legend is the same as in Fig. 3, except that the *dotted blue line* 6 indicates the population of the reduced external acceptor Cl_2NQ

Discussion

Midpoint redox potentials of electron acceptors

Forward and backward ET reactions in PS I complexes are controlled by redox potentials of cofactors (see Fig. 1; Table 3). The terminal electron acceptors in PS I are Fe–S clusters, F_A and F_B, and their midpoint redox potentials (E_m) were determined as −500 mV and −550 mV versus SHE, respectively (Golbeck et al. 1987). The midpoint potential of F_X was approx. 200 mV lower (Chamorovsky and Cammack 1982; Parrett et al. 1989), and the operating potential of A_1 was too low for direct experimental determination and therefore was calculated to be between

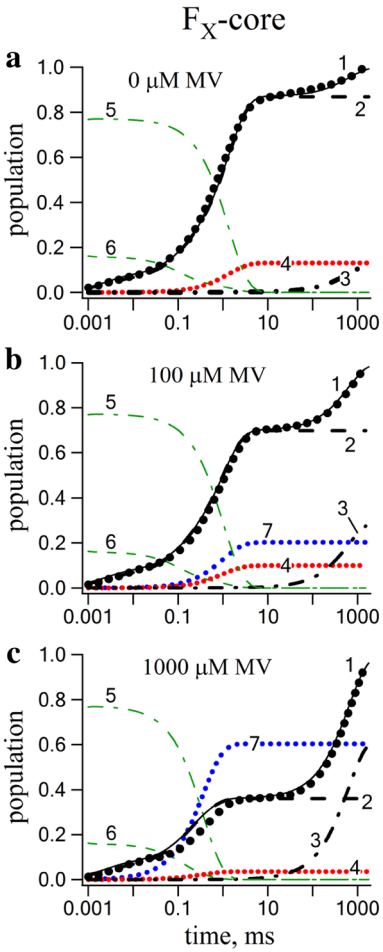

Fig. 5 Effect of MV on the P_{700}^+ reduction in F_X-core of PS I. The legend is the same as that given in Fig. 3; in addition, population of reduced internal cofactor A_{1A} is shown by *green dashed line* 6 (contribution of reduced A_{1B} is less than 5% and is not shown), and that of the reduced external acceptor MV is shown by *blue dotted line* 7

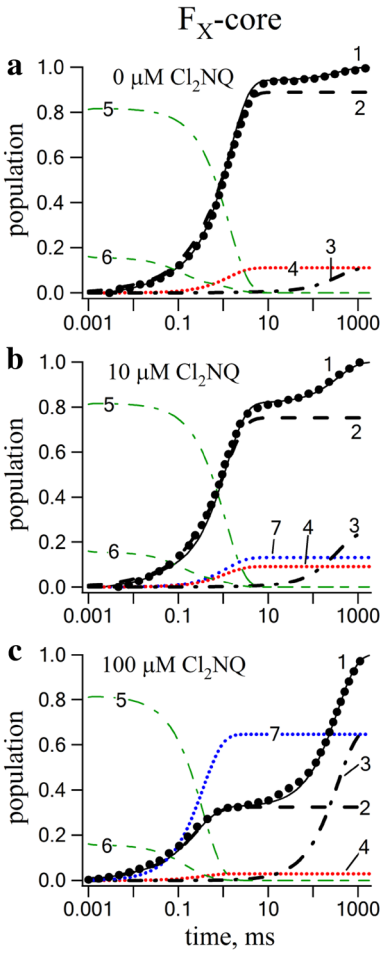

Fig. 6 Effect of Cl_2NQ on the P_{700}^+ reduction in F_X-core of PS I. The legend is the same as in Fig. 3, except that the *dotted blue line* 7 indicates the population of the reduced external acceptor Cl_2NQ

−585 mV (Ptushenko et al. 2008) and −810 mV (Vos and van Gorkom 1990).

As it is impossible to measure the E_m of quinones bound to A_1-sites in PS I directly, it seems reasonable to compare it to the values measured in aprotic solvent dimethylformamide (DMF), chemical properties of which resemble protein environment of quinone-binding sites. The measured E_m values of PhQ, PQ, and Cl_2NQ in DMF versus SCE are summarized in the middle column of Table 3. The high-potential Cl_2NQ is used in this study in two different ways. This quinone was either incorporated into PS I instead of PhQ, or it was used as an external acceptor dissolved in water. In the latter case, the E_m of Cl_2NQ in water characterizes its efficiency, together with potentials of other acceptors – MV and molecular oxygen (Table 3). For comparison, the E_m values of 2,3-dimethyl-naphthoquinone and 2,3,5-trimethyl-benzoquinone (soluble analogs of PhQ and PQ) in water are also presented. In this study, we have estimated the E_m values of low-potential redox cofactors, including two quinones in the A_{1A}-site and iron–sulfur cluster, F_X (Table 3).

ET reactions in PS I of WT

The main kinetic component of P_{700}^+ recombination in PS I complexes of WT in the absence of native external acceptor ferredoxin (*Fd*) or flavodoxin (*Fld*) has the characteristic time of 50 ms, while faster components of recombination have too small amplitude to be resolved (Fig. 3a). The main component arises due to ET from the iron–sulfur clusters $[F_A/F_B]^-$ (Vassiliev et al. 1997) occurring by two alternative channels: via the internal recombination with P_{700}^+ (Makita et al. 2015) and by the external reaction with molecular oxygen (Trubitsin et al. 2014), which have similar rates $k_{30}=7.6\ s^{-1}$ and $k_{O2}=15\ s^{-1}$ in our experimental conditions (see Tables 1, 2). The contributions of both

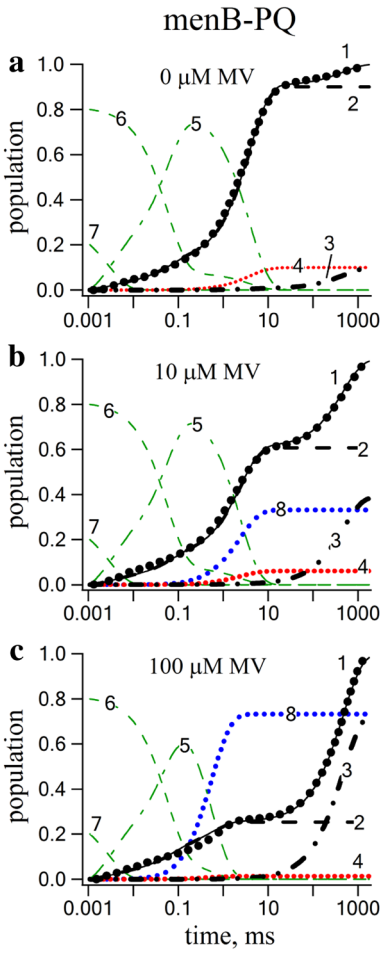

Fig. 7 Effect of MV on P_{700}^+ reduction kinetics in *menB*-PQ. The legend is the same as that given in Fig. 3; in addition, populations of reduced internal cofactors are shown by *green lines: dash-dotted line* 5 for iron–sulfur clusters, *dashed lines* 6 and 7 for A_{1A} and A_{1B}, respectively; the reduced external acceptor MV is shown by *blue dotted line* 8

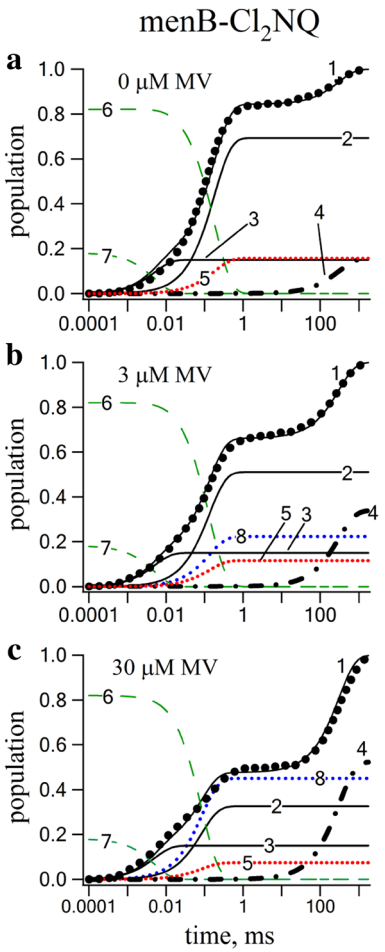

Fig. 8 Effect of MV on P_{700}^+ reduction kinetics in *menB*-Cl_2NQ. Curves notation: experimental P_{700} recovery kinetics (*black dots*, 1), modeled P_{700} recovery kinetics (*black solid line*, 1); the fraction of P_{700} population, reduced by A_{1A} (*black solid line*, 2), A_{1B} (*black solid line*, 3) and by external donor DCPIP (*black dash-dotted line*, 4); the reduced external oxygen (*red dotted line*, 5); the populations of reduced A_{1A} (thin *green* dashed *line*, 6) and A_{1B} (thin *green* dashed *line*, 7); and the reduced external MV (*blue dotted line*, 8)

reactions (about 40 and 60%) are shown by black dashed line 2 and red dotted line 4 in Fig. 3, respectively. In the complexes where electron was captured by oxygen, P_{700}^+ was reduced by DCPIP with $k_{donor} = 1.5\ s^{-1}$ (black dash-dotted line 3 in Fig. 3).

Due to a very large distance between F_A/F_B and P_{700} (>40 Å), the electron is transferred to P_{700}^+ through intermediate cofactors including the preceding acceptor F_X and probably A_{1A} (Fig. 1). According to Eq. 4, the rate constant k_{30} of ET from $[F_A/F_B]^-$ to P_{700}^+ is a product $(K_{12A} \times K_{23})^{-1} \times k_{10A}$. The recombination rate constant k_{10A} was determined in modified PS I preparations: in complexes depleted with F_X and F_A/F_B clusters (Brettel and Golbeck 1995; Shen et al. 2002) and with high-potential Cl_2NQ incorporated into the site A_1 (Makita and Hastings 2015); in both cases, the rate constant k_{10A} has a value of $10^4\ s^{-1}$. We determined $k_{10A} = 9 \times 10^3\ s^{-1}$ in a small fraction of impaired F_X-core complexes (Fig. 5; Table 1), and using this value yielded the estimate of the product $K_{12A} \times K_{23}$ as 1.2×10^3.

In the presence of MV, the oxidation of $[F_A/F_B]^-$ was accelerated by increasing the concentration of acceptor: at 10 μM, MV captured more than 90% of electrons, so the P_{700}^+ reduction was achieved mainly by donation from external electron donor DCPIP (dash-dotted line 3 in Fig. 1c). Because the reduction of P_{700}^+ by $[F_A/F_B]^-$ clusters decreased in the presence of MV, we could not determine the dissociation constant K_m of MV interaction with PS I. The bimolecular rate constant of MV interaction with $[F_A/F_B]^-$, k_a, was estimated as $1.6 \times 10^7\ M^{-1}\ s^{-1}$ (Table 2).

The interaction of Cl_2NQ as external acceptor with PS I differs from that of MV. First, the bimolecular rate constant

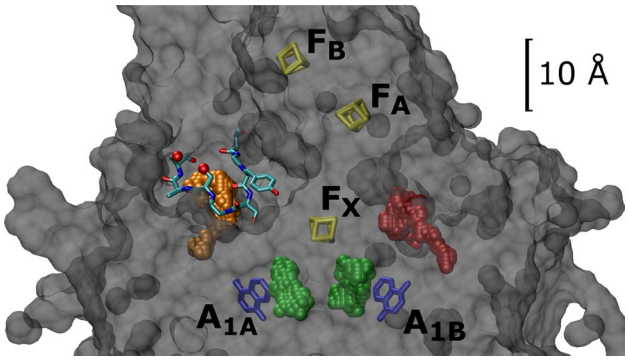

Fig. 9 Protein cavities in the vicinity of A_1-binding sites in PS I. The quinones A_{1A} and A_{1B} are shown in *blue*; and iron–sulfur clusters F_X, F_A, and F_B – in *yellow*. Surface of PS I cross section, containing these cofactors, is shown in gray. Four cavities are shown as *colored spheres*: internal water-filled cavities between A_1 and F_X (*green*) and near-surface cavities in the vicinity of A_1-sites (*orange* and *red* for A_{1A} and A_{1B}, respectively). The loop of the protein subunit *E*, framing the *A*-side cavity on the protein surface, is shown as wireframe; two hydroxyl groups, presumably localized at the mouth of the cavity, are shown as *red spheres*

of Cl_2NQ interaction with WT PS I was higher, 1.1×10^8 M^{-1} s^{-1} (Table 2). Second, Cl_2NQ binds to PS I with a moderate affinity with the dissociation constant $K_m = 5$ μM, which is typical for nonspecific binding of polar organic compounds at protein-water interface.

For comparison, we also included in Table 2 data characterizing the interaction of PS I with native external acceptors *Fd* and *Fld*, small soluble proteins, which bind specifically at the acceptor side of PS I (Sétif 2001). It is worth noting that the efficiency of Cl_2NQ is higher than that of *Fld* and is only threefold smaller than the efficiency of *Fd*. Presumably, the high electron-accepting activity of Cl_2NQ is a result of high mobility, polar chemical properties, and the high redox potential of this compound (Table 3).

It is worthwhile to compare the efficiency of MV and Cl_2NQ with molecular oxygen dissolved in water. Because the concentration of molecular oxygen in water is ~2×10^{-4} M, the bimolecular rate constant of O_2 interaction with reduced [F_A/F_B] clusters is 7.5×10^4 M^{-1} s^{-1}. This reaction is relatively slow compared to the interactions with MV, Cl_2NQ, and native protein acceptors, *Fd* and *Fld* (Table 2). Nevertheless, the reduction of oxygen as byproduct of PS I functioning might be important source of superoxide-radical in photosynthesizing organisms (see below).

ET reactions in F_X-core complexes

The removal of F_A/F_B clusters by the urea treatment of PS I complexes (F_X-core) resulted in a significant acceleration of recombination kinetics (Fig. 5). In the absence of exogenous acceptors, the main kinetic component (~80%) is attributable to the backward reaction from F_X^- to P_{700}^+ with $\tau \approx 1$ ms, which is in line with the previously obtained data for $P_{700}^+F_X^-$ recombination (Vassiliev et al. 1997; Shinkarev et al. 2000; Shen et al. 2002). In these preparations, fast kinetic components (τ of 3–100 μs, total amplitude of ~17%) are also observed, which could be ascribed to charge recombination from the quinone acceptors, A_{1A} and A_{1B}, in a fraction of F_X-core complexes with depleted F_X cluster (Shen et al. 2002). The rate constants of these components are estimated as 9.1×10^3 and 4.0×10^5 s^{-1}, respectively (Table 1), which are close to the previous estimates (Brettel and Golbeck 1995; Shen et al. 2002; Makita and Hastings 2015). In the remaining 10% centers, electron is captured by molecular oxygen $k_{O_2} = 250\,s^{-1}$, and the slow reduction of P_{700}^+ by DCPIP is observed.

The charge recombination in F_X-core complexes provides additional information on ET reactions at the acceptor side of PS I. A comparison of the recombination kinetics in WT PS I and F_X-core allows us to

Table 3 Midpoint redox potential values of various electron acceptors

Acceptor	E_m in water (SHE), mV	E_m in DMF (SCE), mV	This study (SHE), mV
PhQ	−240[a,n]	−710[i]	
PQ	−165[a,n]	−620[i]	
Cl_2NQ	−98[b]	−400[j]	
MV	−448[a]		
O_2	−155[a]		
Fd	−412[c]		
F_AF_B	−500[d]		−500[d]
F_X	−670[e], −705[f]		−630[m]
A_{1A} (PhQ)	−670[g], −810[h]		−680[m]
A_{1B} (PhQ)	−840[g]		−850[l]
A_{1A}(PQ)	−560[k]		−555[m]

[a]Wardman (1989)

[b]Currie and Holmes (1966)

[c]Bottin and Lagoutte (1992)

[d]Golbeck et al. (1987)

[e]Parrett et al. (1989)

[f]Chamorovsky and Cammack (1982)

[g]Ptushenko et al. (2008)

[h]Vos and van Gorkom (1990)

[i]Prince et al. (1983)

[j]Shalev and Evans (1989); Ibis et al. (2015)

[k]Makita and Hastings (2016)

[l]Values based on E_m of A_{1A}, obtained in this study, and E_m difference of −170 mV between A_{1B} and A_{1A}, taken from Ptushenko et al. (2008)

[m]Values derived from equilibrium constants obtained in this study

[n]Data for water-soluble analogs of PhQ and PQ, 2,3-dimethyl-naphthoquinone and 2,3,5-trimethyl-benzoquinone are presented

estimate the equilibrium constant between F_A/F_B and F_X clusters. Since recombination from $[F_A/F_B]^-$cluster occurs through intermediate F_X-reduced state, the acceleration of recombination by a factor of 170 from 7.6 s^{-1} in WT to 1.3×10^3 s^{-1} in F_X-core complexes corresponds to the redox potential difference of 130 mV between F_A/F_B and F_X. The midpoint potential of F_X cluster $E_m(F_X)=-630$ mV could be thus calculated from the directly measured midpoint potential of F_A/F_B (Table 3). This estimate is more positive than the values of −670 or −705 mV, obtained by direct redox titration (Chamorovsky and Cammack 1982; Parrett et al. 1989), but more negative than the calculated operating E_m value of −585 mV (Ptushenko et al. 2008). This difference seems to be meaningful because F_X redox titration in the intact PS I occurs under equilibrium conditions, when the nearby reduced F_A and F_B clusters lower the potential of F_X by electrostatic effect of their two negative charges. As calculated previously, this electrostatic effect has a magnitude of −70 mV (Ptushenko et al. 2008). Similar shift of the equilibrium midpoint potential $E_m(F_X)$ by 60 mV was found in F_X-core complexes, where F_A and F_B clusters were absent (Parrett et al. 1989). On the other hand, the analysis of recombination kinetics yields the operating energy gap between F_X and F_A/F_B clusters, which characterizes the potential of F_X in conditions, where F_A and F_B are both oxidized, so the value of −630 mV is a reasonable estimate of the operating $E_m(F_X)$ value consistent with the experimental data.

Addition of the external acceptor MV leads to acceleration of the millisecond P_{700}^+ reduction component, with simultaneous decrease of its amplitude and increase of amplitude of the slow component associated with P_{700}^+ reduction by an external donor (Fig. 5b, c). The kinetics of P_{700}^+ reduction in the time range of 3–30 μs did not change. The bimolecular rate constant of F_X cluster oxidation by external acceptor MV was approximately 3× lower than the rate constant of $[F_A/F_B]$ oxidation in the WT PS I (Table 2). At the same time, dependence of the oxidation rate on MV concentration did not exhibit saturation effect even at the highest acceptor concentration of 1 mM. This suggests that both F_X and F_A/F_B clusters are oxidized by external acceptor MV at the polar interface of the complex without any specific MV-binding site.

The interaction of Cl_2NQ with F_X-core was different compared with the WT PS I: while in WT, we observed Cl_2NQ binding with the affinity, $K_m=5$ μM, in F_X-core, we did not observe further increase of the slow kinetic component due to the forward ET to Cl_2NQ even at 100 μM concentration of the acceptor (Table 2).

ET reactions in the *menB* modification of PS I

The recombination kinetics in the PS I complexes with PQ substituted for the native PhQ (*menB*-PQ) has two significant differences from the WT kinetics. First, the main recombination component is accelerated from 100 ms in the WT up to 3 ms in *menB*-PQ (Table 1; Figs. 3, 7). Second, two additional recombination components with the characteristic times of 10 and 100 μs appear in these complexes. Both these effects can be explained by the fact that the redox potential of the semiquinone/quinone couple is ~100 mV more positive in the case of PQ compared with the native PhQ (Table 3). More positive potential of PQ in the A_{1A}-and A_{1B}-sites leads to slower rates of forward ET to F_X cluster (k_{12A} and k_{12B} decreased by two orders of magnitude from $5\times10^6/5\times10^7$ s^{-1} in the WT complexes to $1.4\times10^4/3\times10^5$ s^{-1} in *menB*-PQ) and to a fifty-fold acceleration of recombination from the terminal F_A/F_B clusters ($k_{30}=325$ s^{-1}), inasmuch as the latter involves the intermediate reduction of quinone in the A_{1A}-site. Concurrently, the PQ/PhQ substitution alters significantly all basic parameters of the model. The equilibrium constant K_{12A} decreases by a factor of 140, which corresponds to ΔG decrease by ~125 mV, in good agreement with PQ/PhQ redox potential difference in DMF (see Table 3). The recombination rate constants k_{10A} and k_{10B} decrease by factors of 3.6 and 8, respectively. Two components of semiquinone re-oxidation in the PQ-substituted complexes with the lifetimes of $\sim2\times10^{-5}$ and $\sim4\times10^{-4}$ s, respectively, and comparable amplitudes were observed by combinations of three different methods (Semenov et al. 2000); similar components were observed in P_{700}^+ recombination kinetics in PQ-substituted PS I complexes both for F_X-core and complexes fully depleted with iron–sulfur clusters (Shinkarev et al. 2002), which is in good agreement with our data. Deceleration of semiquinone oxidation in the A_1-sites by a factor of 200–300 can be caused by various factors: the decrease of driving force by ~130 meV for the forward reactions; the larger effective distance between A_{1A} and F_X due to smaller size of the quinone ring (benzoquinone vs. naphthoquinone); the higher reorganization energy due to the increased conformational mobility and the smaller size of PQ. The dynamics of PQ oxidation in the A_{1A}- and A_{1B}-sites (Fig. 7) correspond to the published kinetics for similar modified complexes of PS I (Semenov et al. 2000; Shinkarev et al. 2002).

ET reactions in the *menB* modification of PS I with substituted Cl_2NQ

The recombination kinetics in the PS I complexes with Cl_2NQ substituted for the native *PhQ* (*menB*-Cl_2NQ) were significantly faster than in the WT (Fig. 8). The midpoint

potential of Cl_2NQ in DMF is ~300 mV more positive than that of PhQ (Table 3), which places Cl_2NQ midpoint potential in the A_{1A}-site higher than −400 mV. Thereby the electron equilibrium between terminal acceptors in this modification of PS I is heavily biased in favor of the A_{1A}-site. Thus, the main component of recombination kinetics in this case represents a direct ET from A_{1A} to P_{700}^+, the respective rate constant k_{10A} was found to be 9.3×10^3 s^{-1}, which is close to the previously obtained value of 7×10^3 s^{-1} (Makita and Hastings 2015). The faster component of recombination in these complexes has the rate constant of 2.8×10^5 s^{-1} and the amplitude of 14–17%, which is also in accordance with the data by (Makita and Hastings 2015) who assigned this reaction to the ET from A_{1B} to P_{700}^+.

The bimolecular rate constant of Cl_2NQ oxidation by external acceptor MV in the A_1-site is as high as 1.5×10^9 M^{-1} s^{-1} (Table 2). Such remarkable efficiency is close to the limit of diffusion-controlled reactions (Eigen and Hammes 2006). The quinone-binding site A_1 is also efficiently interacting with molecular oxygen: in the absence of external acceptor, about 10% of electrons in the PS I complexes with Cl_2NQ in the site A_1 are captured by oxygen (Fig. 8), which corresponds to the rate constant $k_{O_2} = 10^3$ s^{-1}.

Production of reactive oxygen species in PS I

PS I can reduce molecular oxygen (O_2) and produce superoxide radical ($O_2^{\bullet-}$) and other forms of reactive oxygen species (ROS) via the Mehler reaction (Mehler 1951; Badger et al. 2000). The internal cofactors of the PS I acceptor side are considered as the major O_2-reducing agents in chloroplasts, but in spite of the long history, there is no consensual view on the mechanism of oxygen reduction at the acceptor side of PS I (Ivanov and Khorobrykh 2003; Asada 2006). The present kinetic model allows quantitative characterization of the oxygen-reduction activity of internal cofactors in the PS I acceptor side.

The effective rate constant of oxygen reduction by terminal clusters F_A and F_B in WT PS I is $k_{O2}=15$ s^{-1}, whereas the typical rates of *Fd* reduction in vitro are of the order of 10^6 s^{-1} (Sétif 2001). It means that the probability of O_2 reduction by $[F_A/F_B]$ is ~10^{-5} compared to the probability of *Fd* reduction. The rate constant of O_2 reduction by F_X in WT remains unknown, but in F_X-core complexes, it was determined as $k_{O_2} = 250$ s^{-1}. Comparison of this value with the ET rate between F_X and $[F_A/F_B]$ clusters $k_{23}=10^7$ s^{-1} yields the similar probability of side ROS production of 2×10^{-5}. The highest rate $k_{O2}=10^3$ s^{-1} was determined for oxygen reduction by Cl_2NQ in the A_1-site of *menB*-Cl_2NQ complexes, where electron was trapped by O_2 before recombination with P_{700}^+. Because E_m of PhQ in the A_1-site is presumably ~300 mV lower than the E_m value of Cl_2NQ (see Table 3), the rate of O_2 reduction by A_1 in WT PS I should be at least an order of magnitude higher, i.e., 10^4 s^{-1}. Considering the rate of forward ET from A_1 to F_X in WT as 3×10^6 s^{-1} (Agalarov and Brettel 2003), this leads to at least 0.3% probability of the superoxide-radical production, bypassing terminal acceptors of PS I. The direct indication on the role of phylloquinone in the A_1-site as a sink of electrons for the oxygen reduction in PS I was demonstrated previously by measurements of O_2 uptake with Clark electrode (Kozuleva et al. 2014). It was also shown that the oxygen reduction at the acceptor side of PS I provides an alternative channel for electron flow in plant chloroplasts under conditions of low electron acceptor efficiency (Kuvykin et al. 2011). Oxygen is a main product of photosynthesis reaction in plants; so, for the efficient functioning of PS I, it is important to prevent its interaction with the cofactors of ET chain. The high rate of side reactions of low-potential PhQ in the A_1-site might rationalize the presence of the less-reactive 4Fe–4S clusters as terminal acceptors, which are reduced by A_1 within 10^{-6} s after excitation of P_{700}.

Energetics of ET reactions in the acceptor side of PS I

The kinetic efficiency of ET between donor D and acceptor A in a protein complex is determined by three basic parameters: the energy of electronic coupling, H_{DA}; the free energy change of reaction, ΔG_{DA}; and the reorganization energy of cofactors recharging, λ (Krishtalik 2016). In PS I, the distance between PhQ in the sites A_{1A}/A_{1B} and F_X is 9 Å (Jordan et al. 2001). This distance corresponds to the electronic coupling H_{DA} of 10 cm^{-1} and to the driving-force-optimized tunneling rate of 10^{10} s^{-1} (Winkler and Gray 2014). The optimal ET rate is achieved when the driving force is equal to the reorganization energy ($-\Delta G=\lambda$); in this case ,the activation energy of ET reaction $E^a = (\Delta G + \lambda)^2/4k_BT$ is zero. However, uncertainty in determination of these parameters for ET reactions at the acceptor side of PS I is large. Particularly, when the errors in the estimation of electronic coupling factor H_{DA} by the distance between cofactors exceed an order of magnitude, the redox potential of A_1 could not be measured directly, and the reorganization energy of $A_1 \rightarrow F_X$ ET could be only roughly estimated using the data for similar systems. The reorganization energy for ET from $[4Fe–4S]^{2+}$ cluster to ruthenium–bipyridine–histidine complex in high-potential iron–sulfur protein was determined to be in the range of 0.6–0.9 eV (Babini et al. 2000), and the inner-sphere reorganization energy $\lambda=0.64$ eV for [4Fe–4S] cluster in ferredoxin was obtained by DFT calculations (Sigfridsson et al. 2001). The reorganization energy for PhQ charging in the A_1-site might be estimated by charge recombination in the photosynthetic bacterial reaction center where quinone

moiety in the Q_A-site was altered by various substitutions, and the value of 0.6 eV was determined (Dutton and Mosser 1994). Because the dielectric permittivity of PS I in the acceptor side between A_1 and F_X is higher than the local permittivity of the site Q_A (Chamorovsky et al. 2007), the lowest estimate for reorganization energy of $A_1 \rightarrow F_X$ reaction is $\lambda = 0.7$ eV. This value was suggested by Makita and Hastings 2016 as consistent with the data on quinone substitutions in the A_1-site. The temperature dependence of $A_1 \rightarrow F_X$ reaction in PS I from *Synechocystis* sp. PCC 6803 revealed the presence of two kinetic components: the first component ($\tau = 11$ ns at 295 K) was temperature independent, and the second component ($\tau = 340$ ns at 295 K) slowed upon cooling with an activation energy $E^a = 110$ meV; they were assigned to ET in the branches, A and B, respectively (Agalarov and Brettel 2003). Because the activation energy is a reliably measurable parameter, it is worthy to relate the measured temperature dependencies with the predictions from kinetic models.

In the pioneer work (Shinkarev et al. 2002), the energy gap for the $A_1 \rightarrow F_X$ transition $\Delta G_1 = -100$ meV was calculated without discrimination of the reaction pathways in the branches, *A* and *B* (Model 1). More recent works accounted for the two ET channels and yielded the estimates $\Delta G_{1A} = +16$ meV for the *A* branch and $\Delta G_{1B} = -19$ meV for the *B* branch (Santabarbara et al. 2005) (Model 2), and $\Delta G_{1A} = +45$ meV and $\Delta G_{1B} = -10$ meV (Makita and Hastings 2016) (Model 3). In the present work, we obtained higher estimates of the driving forces for both channels: $\Delta G_{1A} = -50$ meV and $\Delta G_{1B} = -220$ meV (Model 4). The estimate $\Delta G_1 = -100$ meV in Model 1 might be considered as an average value between $\Delta G_{1A} = -50$ meV and $\Delta G_{1B} = -220$ meV, taking into account that channels *A* and *B* are mixed in the proportion 80:20. Taking the estimate for reorganization energy of $A_1 \rightarrow F_X$ transition $\lambda = 0.7$ eV, we calculate the activation energy E^a of this reaction in both braches, *A* and *B*, to compare these models with experimental data. Model 2 predicts the activation energy $E_{1A}{}^a = 170$ meV for $A_{1A} \rightarrow F_X$ transition, whereas Model 3 gives the value $E_{1A}{}^a = 200$ meV, and the present work yields lower value $E_{1A}{}^a = 150$ meV, which is closer to the experimental value of 110 meV (Agalarov and Brettel 2003). Concerning the transition $A_{1B} \rightarrow F_X$ in branch *B*, all models predict nonzero values for the activation energy. The highest estimate $E_{1B}{}^a = 170$ meV follows from Model 3, a similar value of 165 meV is predicted by Model 2, and the lowest activation energy $E_{1B}{}^a = 80$ meV follows from Model 4, which is more consistent with the activationless regime of $A_{1B} \rightarrow F_X$ transition in branch *B* observed by Agalarov and Brettel (2003). Thus, the parameters obtained by Model 4 provide more reasonable approximation to the kinetics of ET reactions between A_{1A}/A_{1B}-sites and F_X, albeit this model underestimates the free energy gaps in both branches. Such underestimation might be a result of protein impairment after removal of subunit *PsaC* from PS I, since the respective free energy gap was obtained by comparison of WT and F_X-core PS I complexes (Table 1).

Conclusions

The kinetic model of ET reactions in the various PS I complexes based on the analysis of $P_{700}{}^+$ reduction kinetics and the published data was developed. The model describes the ET between the primary donor P_{700}, secondary quinone acceptor A_1, iron–sulfur clusters F_X, F_A/F_B, and external electron acceptors – MV, Cl_2NQ, and molecular oxygen. The rate and equilibrium constants of partial ET reactions in PS I from the WT, *menB*, and F_X-core complexes were derived from the model. The model analysis suggests the following conclusions:

1. The charge recombination between the iron–sulfur clusters $[F_A/F_B]^-$and $P_{700}{}^+$ and between $F_X{}^-$ and $P_{700}{}^+$ occurs via preceding acceptor quinone in the A_1-binding site.
2. The obtained equilibrium constants of ET in PS I allow estimating the free energy gap ΔG between the redox cofactors. In the WT, ΔG^0 between the iron–sulfur centers F_X and F_A/F_B is estimated as −130 meV, ΔG^0 between the secondary quinone acceptor A_1 in the branch *A* and F_X is −50 meV. The corresponding ΔG^0 between A_{1A} and F_X for PQ in the PS I from *menB* strain is +75 meV, creating energy barrier for ET to terminal acceptors F_A/F_B. The redox potential of Cl_2NQ in the A_{1A}-site is more positive than −400 mV, fully preventing ET to terminal acceptors.
3. The results obtained for PS I complex containing Cl_2NQ in the A_1-site suggest that the external acceptor MV is capable of accepting electrons directly from A_1, bypassing the iron–sulfur clusters. However, due to the low K_m value, this forward ET reaction could not effectively compete with charge recombination from $A_1{}^-$ to $P_{700}{}^+$ even at high concentration of Cl_2NQ.
4. The rate of interaction of external acceptors MV and O_2 with Cl_2NQ in the A_1-site was found to be high, approaching the limit of diffusion-controlled reactions for MV. The side production of superoxide radical in the A_1-binding site by oxygen reduction (the Mehler reaction) comprises ≥0.3% of the total electron flow in PS I. The existence of highly efficient ET to iron–sulfur clusters in PS I may serve as an evolutionary implementation against such bypassing.
5. The second-order rate constants k_{ext} and dissociation constants K_m of various PS I complexes with MV and Cl_2NQ were estimated. It was demonstrated that

the values of k_{ext} for ET from PS I to MV for the WT and *menB* strain are similar, but this value is ~3 times lower in F_X-core complexes. The values of k_{ext} for ET from the WT PS I and F_X-core to Cl_2NQ were ~8 times higher than the corresponding k_{ext} values of ET to MV, but the affinity of WT PS I to Cl_2NQ was rather low.

Acknowledgements The authors would like to thank Dr. Mahir Mamedov for valuable discussion. This work was financially supported by the Russian Foundation for Basic Research (Grant 15-04-04252) and the Russian Science Foundation (Grant 14-14-00789).

References

Agalarov R, Brettel K (2003) Temperature dependence of biphasic forward electron transfer from the phylloquinone(s) A1 in photosystem I: only the slower phase is activated. Biochim Biophys Acta 1604:7–12. doi:10.1016/S0005-2728(03)00024-0

Asada K (2006) Production and scavenging of reactive oxygen species in chloroplasts and their functions. Plant Physiol 141:391–396. doi:10.1104/pp.106.082040

Babini E, Bertini I, Borsari M et al (2000) Bond-mediated electron tunneling in ruthenium-modified high-potential iron–sulfur protein. J Am Chem Soc 122:4532–4533. doi:10.1021/ja994472t

Badger MR, von Caemmerer S, Ruuska S, Nakano H (2000) Electron flow to oxygen in higher plants and algae: rates and control of direct photoreduction (Mehler reaction) and rubisco oxygenase. Philos Trans R Soc B 355:1433–1446. doi:10.1098/rstb.2000.0704

Bottin H, Lagoutte B (1992) Ferrodoxin and flavodoxin from the cyanobacterium Synechocystis sp PCC 6803. Biochim Biophys Acta 1101:48–56. doi:10.1016/0167-4838(92)90465-P

Brettel K, Golbeck JH (1995) Spectral and kinetic characterization of electron acceptor A1 in a Photosystem I core devoid of iron–sulfur centers FX, FB and FA. Photosynth Res 45:183–193. doi:10.1007/BF00015559

Brettel K, Leibl W (2001) Electron transfer in photosystem I. Biochim Biophys Acta 1507:100–114. doi:10.1016/S0005-2728(01)00202-X

Chamorovsky SK, Cammack R (1982) Direct determination of the midpoint potential of the acceptor X in chloroplast photosystem by electrochemical reduction and ESR spectroscopy. Photobiochem Photobiophys 4:195–200

Chamorovsky SK, Cherepanov DA, Chamorovsky CS, Semenov AY (2007) Correlation of electron transfer rate in photosynthetic reaction centers with intraprotein dielectric properties. Biochim Biophys Acta 1767:441–448. doi:10.1016/j.bbabio.2007.01.008

Currie DJ, Holmes HL (1966) Polarographic Half-wave potentials of some 1,4-naphthoquinones. Can J Chem 44:1027–1029. doi:10.1139/v66-152

Díaz-Quintana A, Leibl W, Bottin H, Sétif P (1998) Electron transfer in photosystem I reaction centers follows a linear pathway in which iron–sulfur cluster FB is the immediate electron donor to soluble ferredoxin. BioChemistry 37:3429–3439. doi:10.1021/bi972469l

Dutton PL, Mosser CC (1994) Quantum biomechanics of long-range electron transfer in protein: hydrogen bonds and reorganization energies. Proc Natl Acad Sci USA 91:10247–10250. doi:10.1073/pnas.91.22.10247

Dutton PL, Page CC, Moser CC, Chen X (1999) Natural engineering principles of electron tunnelling in biological oxidation|[ndash]|reduction. Nature 402:47–52. doi:10.1038/46972

Eigen M, Hammes GG (2006) Elementary steps in enzyme reactions (as studied by relaxation spectrometry). Wiley, Hoboken, NJ

Fehlberg E (1970) Klassische runge-kutta-formeln vierter und niedrigerer ordnung mit schrittweiten-kontrolle und ihre anwendung auf wärmeleitungsprobleme. Computing 6:61–71. doi:10.1007/BF02241732

Fromme P, Mathis P (2004) Unraveling the Photosystem I reaction center: a history or the sum of many efforts. Photosynth Res 80:109–124. doi:10.1023/B:PRES.0000030657.88242.e1

Golbeck JH, Parrett KG, McDermott AE (1987) Photosystem I charge separation in the absence of center A and B. III. Biochemical characterization of a reaction center particle containing P-700 and FX. BBA 893:149–160. doi:10.1016/0005-2728(87)90034-X

Guergova-Kuras M, Boudreaux B, Joliot A et al (2001) Evidence for two active branches for electron transfer in photosystem I. Proc Natl Acad Sci USA 98:4437–4442. doi:10.1073/pnas.081078898

Hopfield JJ (1974) Electron transfer between biological molecules by thermally activated tunneling. Proc Natl Acad Sci 71:3640–3644. doi:10.1073/pnas.71.9.3640

Ibis C, Shntaif H, Bahar H, Ayla S (2015) An investigation of nucleophilic substitution reactions of 2,3-dichloro-1,4-naphthoquinone with various nucleophilic reagents. J Serbian Chem Soc 80:731–738. doi:10.2298/JSC141124021I

Ishikita H, Knapp E-W (2003) Redox potential of quinones in both electron transfer branches of photosystem I. J Biol Chem 278:52002–52011. doi:10.1074/jbc.M306434200

Ivanov B, Khorobrykh S (2003) Participation of photosynthetic electron transport in production and scavenging of reactive oxygen species. Antioxid Redox Signal 5:43–53. doi:10.1089/152308603321223531

Jordan R, Nessau U, Schlodder E (1998) Charge recombination between the reduced iron–sulphur clusters and P700+. In: Garab G (ed) Photosynthesis: mechanisms and effects: volume I Proceedings of the XIth International congress on photosynthesis, Budapest, Hungary, August 17–22, 1998. Springer, Dordrecht, pp 663–666

Jordan P, Fromme P, Witt HT et al (2001) Three-dimensional structure of cyanobacterial photosystem I at 2.5A resolution. Nature 411:909–917. doi:10.1038/35082000

Jortner J (1976) Temperature dependent activation energy for electron transfer between biological molecules. J Chem Phys 64:4860. doi:10.1063/1.432142

Kozuleva MA, Petrova AA, Mamedov MD et al (2014) O2 reduction by photosystem I involves phylloquinone under steady-state illumination. FEBS Lett 588:4364–4368. doi:10.1016/j.febslet.2014.10.003

Krishtalik LI (2016) Fundamentals of electron transfer in proteins. In: Cramer AW, Kallas T (eds) Cytochrome complexes: evolution, structures, energy transduction, and signaling. Springer, Dordrecht, pp 73–98

Kuvykin I V., Ptushenko V V., Vershubskii A V., Tikhonov AN (2011) Regulation of electron transport in C3 plant chloroplasts in situ and in silico: Short-term effects of atmospheric CO_2 and O_2. Biochim Biophys Acta 1807:336–347. doi:10.1016/j.bbabio.2010.12.012

Makita H, Hastings G (2015) Directionality of electron transfer in cyanobacterial photosystem I at 298 and 77 K. FEBS Lett 589:1412–1417. doi:10.1016/j.febslet.2015.04.048

Makita H, Hastings G (2016) Modeling electron transfer in photosystem I. Biochim Biophys Acta 1857:723–733. doi:10.1016/j.bbabio.2016.03.015

Makita H, Zhao N, Hastings G (2015) Time-resolved visible and infrared difference spectroscopy for the study of photosystem

I with different quinones incorporated into the A1 binding site. Biochim Biophys Acta 1847:343–354. doi:10.1016/j.bbabio.2014.12.007

Mamedov M, Govindjee, Nadtochenko V, Semenov A (2015) Primary electron transfer processes in photosynthetic reaction centers from oxygenic organisms. Photosynth Res 125:51–63. doi:10.1007/s11120-015-0088-y

Matsuoka T, Tanaka S, Ebina K (2016) Reduced minimum model for the photosynthetic induction processes in photosystem I. J Photochem Photobiol B 160:364–375. doi:10.1016/j.jphotobiol.2016.04.009

Mehler AH (1951) Studies on reactions of illuminated chloroplasts: I. Mechanism of the reduction of oxygen and other hill reagents. Arch Biochem Biophys 33:65–77. doi:10.1016/0003-9861(51)90082-3

Milanovsky GE, Ptushenko V V., Golbeck JH et al (2014) Molecular dynamics study of the primary charge separation reactions in photosystem I: effect of the replacement of the axial ligands to the electron acceptor A0. Biochim Biophys Acta 1837:1472–1483. doi:10.1016/j.bbabio.2014.03.001

Parrett KG, Mehari T, Warren PG, Golbeck JH (1989) Purification and properties of the intact P-700 and Fx-containing photosystem I core protein. Biochim Biophys Acta 973:324–332. doi:10.1016/S0005-2728(89)80439-6

Prince RC, Dutton PL, Bruce JM (1983) Electrochemistry of ubiquinones. Menaquinones and plastoquinones in aprotic solvents. FEBS Lett 160:273–276. doi:10.1016/0014-5793(83)80981-8

Ptushenko VV, Cherepanov DA, Krishtalik LI, Semenov AY (2008) Semi-continuum electrostatic calculations of redox potentials in photosystem I. Photosynth Res 97:55–74. doi:10.1007/s11120-008-9309-y

Santabarbara S, Zucchelli G (2016) Comparative kinetic and energetic modelling of phyllosemiquinone oxidation in Photosystem I. Phys Chem Chem Phys 18:9687–9701. doi:10.1039/C5CP06590A

Santabarbara S, Heathcote P, Evans MCW (2005) Modelling of the electron transfer reactions in photosystem I by electron tunnelling theory: The phylloquinones bound to the PsaA and the PsaB reaction centre subunits of PS I are almost isoenergetic to the iron–sulfur cluster FX. Biochim Biophys Acta 1708:283–310. doi:10.1016/j.bbabio.2005.05.001

Semenov AY, Vassiliev IR, van Der Est A et al (2000) Recruitment of a foreign quinone into the A1 site of photosystem I. Altered kinetics of electron transfer in phylloquinone biosynthetic pathway mutants studied by time-resolved optical, EPR, and electrometric techniques. J Biol Chem 275:23429–23438. doi:10.1074/jbc.M000508200

Setif P, Brettel K (1993) Forward electron transfer from phylloquinone A1 to iron-sulfur centers in spinach photosystem I. Bio-Chemistry 32:7846–7854. doi:10.1021/bi00082a002

Sétif P (2001) Ferredoxin and flavodoxin reduction by photosystem I. Biochim Biophys Acta 1507:161–179. doi:10.1016/S0005-2728(01)00205-5

Sétif P, Mathis P, Vänngård T (1984) Photosystem I photochemistry at low temperature. Heterogeneity in pathways for electron transfer to the secondary acceptors and for recombination processes. BBA 767:404–414. doi:10.1016/0005-2728(84)90038-0

Shalev H, Evans DH (1989) Solvation of anion radicals: gas phase vs solution. J Am Chem Soc 111:2667–2674. doi:10.1021/ja00189a048

Shen G, Antonkine ML, van der Est A et al (2002) Assembly of photosystem I. II. Rubredoxin is required for the in vivo assembly of F(X) in Synechococcus sp. PCC 7002 as shown by optical and EPR spectroscopy. J Biol Chem 277:20355–20366. doi:10.1074/jbc.M201104200

Shinkarev V (2006) Functional modeling of electron transfer in photosynthetic reaction centers. In: Golbeck JH (ed) Photosystem I: the light-driven plastocyanin:ferredoxin oxidoreductase. Springer, Dordrecht, pp 611–637

Shinkarev VP, Vassiliev IR, Golbeck JH (2000) A kinetic assessment of the sequence of electron transfer from FX to FA and further to FB in photosystem I: the value of the equilibrium constant between FX and FA. Biophys J 78:363–372. doi:10.1016/S0006-3495(00)76599-4

Shinkarev VP, Zybailov B, Vassiliev IR, Golbeck JH (2002) Modeling of the P700+ charge recombination kinetics with phylloquinone and plastoquinone-9 in the A1 site of photosystem I. Biophys J 83:2885–2897. doi:10.1016/S0006-3495(02)75298-3

Sigfridsson E, Olsson MHM, Ryde U (2001) Inner-sphere reorganization energy of iron–sulfur clusters studied with theoretical methods. Inorg Chem 40:2509–2519. doi:10.1021/ic000752u

Srinivasan N, Golbeck JH (2009) Protein–cofactor interactions in bioenergetic complexes: The role of the A1A and A1B phylloquinones in photosystem I. Biochim Biophys Acta 1787:1057–1088. doi:10.1016/j.bbabio.2009.04.010

Sun J, Hao S, Radle M et al (2014) Evidence that histidine forms a coordination bond to the A0A and A0B chlorophylls and a second H-bond to the A1A and A1B phylloquinones in M688HPsaA and M668HPsaB variants of Synechocystis sp. PCC 6803. Biochim Biophys Acta 1837:1362–1375. doi:10.1016/j.bbabio.2014.04.004

Tikhonov AN (2016) Modeling electron and proton transport in chloroplasts. In: Kirchhoff H (ed) Chloroplasts: current research and future trends. Caister Academic Press, Norfolk, UK, pp 101–134

Trubitsin BV, Mamedov MD, Semenov AY, Tikhonov AN (2014) Interaction of ascorbate with photosystem I. Photosynth Res 122:215–231. doi:10.1007/s11120-014-0023-7

Vassiliev IR, Jung YS, Mamedov MD et al (1997) Near-IR absorbance changes and electrogenic reactions in the microsecond-to-second time domain in Photosystem I. Biophys J 72:301–315. doi:10.1016/S0006-3495(97)78669-7

Vos MH, van Gorkom HJ (1990) Thermodynamical and structural information on photosynthetic systems obtained from electroluminescence kinetics. Biophys J 58:1547–1555. doi:10.1016/S0006-3495(90)82499-1

Wardman P (1989) Reduction potentials of one-electron couples involving free radicals in aqueous solution. J Phys Chem Ref Data 18:1637. doi:10.1063/1.555843

Winkler JR, Gray HB (2014) Electron flow through metalloproteins. Chem Rev 114:3369–3380. doi:10.1021/cr4004715